Research Square

Preprints are preliminary reports that have not undergone peer review.
They should not be considered conclusive, used to inform clinical practice,
or referenced by the media as validated information.

Chronic Cerebral Small Vessel Disease Burden and Acute Infarction in Relation to Functional Brain Network Efficiency: A Cross-Sectional Resting-State fMRI Study

Yingqi Gao
Lianyungang Clinical College of Nanjing Medical University
Chunqiang Lu
Zhongda Hospital Southeast University
Ying Liu
Lianyungang Clinical College of Nanjing Medical University
Yinan Zhao
Lianyungang Clinical College of Nanjing Medical University
Lijuan Zheng
Zhongda Hospital Southeast University
Yan Gu
guyan2020@njmu.edu.cn

Lianyungang Clinical College of Nanjing Medical University

Research Article

Keywords: cerebral small vessel disease, global efficiency, resting-state fMRI, graph theory, lacune, acute infarction

Posted Date: September 29th, 2026

DOI: https://doi.org/10.21203/rs.3.rs-10978114/v1

License: This work is licensed under a Creative Commons Attribution 4.0 International License.
Read Full License

Additional Declarations: No competing interests reported.

Abstract

Background

Chronic cerebral small vessel disease (CSVD) and acute infarction frequently coexist, but their respective relationships with functional network integration remain uncertain. We examined whether cumulative CSVD burden and clinical acute infarction were independently associated with resting-state functional global efficiency and explored which lesion phenotypes and anatomical regions showed the strongest associations.

Methods

This hospital-based cross-sectional study included 166 patients aged 45 years or older with suspected cerebrovascular disease. Automated multisequence MRI segmentation quantified white matter hyperintensities, recent small subcortical infarcts, lacunes, perivascular spaces, and cerebral microbleeds. Resting-state functional networks were constructed using a 90-region anatomical parcellation, with global efficiency prespecified as the primary outcome. HC3 heteroskedasticity-robust multivariable linear regression adjusted for age, sex, hypertension, diabetes mellitus, mean framewise displacement, and clinical acute infarction. Regional markers were jointly evaluated within each lesion family, with Benjamini-Hochberg false discovery rate correction.

Results

Higher total CSVD burden was independently associated with lower global efficiency (B per 1-point increase = − 0.0055, 95% CI: −0.0086 − 0.0024; P < 0.001), whereas clinical acute infarction was not (B = 0.0008, 95% CI: −0.0071–0.0087; P = 0.850). The lacune regional block explained an additional 9.27% of variance (robust P = 0.00195). Parietal lacunes (B=-0.0130, FDR q = 0.026) and deep lacunes (B=-0.0132, FDR q = 0.021) were independently associated with lower global efficiency. Regional cerebral microbleed, perivascular-space, and white-matter-hyperintensity blocks were not statistically significant.

Conclusions

Greater cumulative CSVD burden, particularly parietal and deep lacunes, was associated with impaired functional network integration, whereas clinical acute infarction showed no independent association in this cohort. These cross-sectional findings identify anatomically informative correlates but do not establish causal or temporal relationships.

Introduction

Cerebral small vessel disease (CSVD) is an umbrella disorder of the brain's small perforating vessels and is expressed on MRI through heterogeneous ischemic, hemorrhagic, and fluid-space abnormalities. STRIVE-2 recognizes recent small subcortical infarcts, lacunes of presumed vascular origin, white matter hyperintensities (WMH), cerebral microbleeds (CMBs), and visible perivascular spaces (PVS), among other features [1–3]. These markers are related but not interchangeable: they differ in tissue substrate, temporal stage, anatomical predilection, and clinical relevance. Moreover, conventional MRI depicts downstream tissue injury rather than small-vessel function itself and therefore captures only part of the underlying disease process [4–6]. Age also strongly influences the expected prevalence and volume of MRI manifestations, complicating the distinction between age-associated change and pathological burden [7].

CSVD can consequently be characterized along several complementary imaging dimensions. Lesion phenotype distinguishes focal cavitation, diffuse white matter injury, prior microscopic hemorrhage, and PVS enlargement; count and volume describe lesion multiplicity and extent; anatomical location indicates whether strategically connected cortical, subcortical, or infratentorial territories are involved; and co-occurrence summarizes cumulative injury across tissue compartments [8]. The widely used 0–4 total CSVD burden score integrates four conventional marker categories and has demonstrated construct validity and generally substantial inter- and intrarater reliability [9, 10]. However, an ordinal score assigns the same weight to each component and compresses potentially important variation in lesion number, volume, and topography. Quantitative multisequence segmentation may retain this information and reduce dependence on coarse visual thresholds [11, 12]. Importantly, lesion location can add biological and clinical information beyond total burden: strategic lacunes have been associated with impaired processing speed [13], and recent multicenter work suggests that the network embedding of WMH predicts cognitive performance better than WMH volume alone [14].

A network framework may help connect these heterogeneous structural lesions to distributed brain dysfunction. In graph theory, global efficiency quantifies the capacity for integrated information transfer across the brain [15]. Structural connectome studies support a CSVD disconnection model in which reduced network efficiency relates to cognitive impairment [16–19]. Resting-state BOLD fMRI extends this framework by measuring functional coupling, with previous studies reporting abnormalities in frontoparietal, default-mode, salience, attention, and cerebellar systems [20–24]. Additional resting-state studies have demonstrated modular reconfiguration, reduced global efficiency, and disrupted default-mode connectivity across CSVD phenotypes [25–28].

Acute infarction introduces an additional source of network disruption through focal tissue injury, diaschisis, and evolving functional reorganization. Acute-stroke studies have reported widespread topological alterations, but estimates vary with lesion location and volume, vascular territory, time from onset, and analytical strategy [29]. Chronic CSVD and acute infarction frequently coexist in clinical cerebrovascular populations. Failure to model both may therefore conflate cumulative small-vessel injury with the acute clinical state, whereas a simple binary acute-infarction indicator cannot fully represent acute lesion heterogeneity.

Against this background, we examined whether total CSVD burden and clinical acute infarction status were independently associated with resting-state functional global efficiency in a mixed hospital cohort, with explicit adjustment for vascular risk factors and head motion. We then used quantitative, anatomically resolved markers to compare regional lacune, CMB, PVS, and WMH families and to estimate their incremental contributions beyond the common covariates. This design was intended to bridge global burden scoring and lesion-specific topography while avoiding causal interpretation of cross-sectional associations. We hypothesized that greater cumulative CSVD burden would be associated with lower global efficiency and that lacunes in strategically connected regions would show location-specific associations.

Materials and methods

Study design and participants

This cross-sectional hospital-based study screened 205 consecutive patients with clinically suspected cerebrovascular disease who underwent conventional brain MRI and resting-state BOLD fMRI at the Department of Radiology, Lianyungang Clinical College of Nanjing Medical University between July 2025 and November 2025. Exclusion criteria were age younger than 45 years (n = 10), incomplete imaging data (n = 9), poor image quality (n = 7), imaging-clinical mismatch or a non-target disorder (n = 4: intracranial space-occupying lesion, n = 2; neuromyelitis optica spectrum disorder, n = 1; non-neurological admission with no cerebrovascular lesion, n = 1), and fewer than 60 retained fMRI time points after head motion censoring (n = 9). The final analytical cohort included 166 participants (Fig. 1), of whom 80 had a clinical acute infarction and 86 did not.

Age, sex, hypertension, and diabetes mellitus were obtained from the study dataset. The protocol was approved by the Lianyungang First People's Hospital Medical Ethics Committee (approval no. KY-20231023001-01). The requirement for written informed consent was waived in accordance with applicable national legislation and institutional requirements. The report was prepared in accordance with general observational neuroimaging reporting principles.

MRI acquisition

MRI was performed using a 3.0-T Signa HD superconducting MR scanner (GE Healthcare) equipped with a dedicated 20-channel head-and-neck coil. The protocol included T1-weighted, T2-weighted, T2-FLAIR, diffusion-weighted imaging with apparent diffusion coefficient maps, susceptibility-weighted imaging, and resting-state BOLD fMRI. Acquisition parameters were as follows: T1-weighted imaging, repetition time (TR)/echo time (TE), 1875/24.0 ms; field of view (FOV), 260 × 260 mm; slice thickness, 5.0 mm; flip angle, 90°; T2-weighted imaging, TR/TE, 7960/102.0 ms; FOV, 260 × 260 mm; slice thickness, 5.0 mm; flip angle, 90°; T2-FLAIR, TR/TE, 8500/220.0 ms; FOV, 260 × 260 mm; slice thickness, 5.0 mm; flip angle, 90°; diffusion-weighted imaging, TR/TE, 5000/75.9 ms; FOV, 260 × 260 mm; slice thickness, 5.0 mm; flip

angle, 90°; b values, 0 and 1000 s/mm²; susceptibility-weighted imaging, TR/TE, 41.0/26.0 ms; FOV, 210 × 210 mm; slice thickness, 4.0 mm; flip angle, 15°; and resting-state BOLD fMRI, TR/TE, 3000/40.0 ms; FOV, 240 × 240 mm; slice thickness, 5.0 mm; flip angle, 90°. A total of 128 time points were acquired for the BOLD sequence. During the resting-state scan, participants were instructed to keep still with eyes closed and breathe calmly.

Quantitative CSVD assessment

CSVD lesions were quantified on a multi-sequence uRP platform using a VB-Net-based automated segmentation workflow, followed by visual review and manual correction by trained readers, consistent with the referenced quantitative method [11]. WMH, RSSI, lacunes, PVS, and CMBs were characterized by lesion number, volume, and anatomical location. WMH volumes were partitioned into juxtaventricular, periventricular, deep, and juxtacortical layers. PVS were assessed by anatomical region, consistent with validated region-specific rating approaches [30]. Regional lacunes and CMBs were represented as presence/absence indicators, whereas regional PVS and WMH volumes were transformed as ln(volume + 1) and standardized within the final 166-participant cohort. The total CSVD burden score ranged from 0 to 4, assigning one point for each prespecified conventional feature category according to the established total-burden approach [9]. All images were independently evaluated by two radiologists with more than 5 years of neuroimaging experience who were blinded to clinical information. Disagreements were resolved by a senior radiologist with more than 20 years of diagnostic experience.

Resting-state fMRI and graph analysis

T1-weighted and resting-state BOLD fMRI data were analyzed automatically using the uAI Research Portal (uRP; Shanghai United Imaging Intelligence Co., Ltd., Shanghai, China) [31]. The first 10 volumes were discarded, followed by head-motion correction. Frames with framewise displacement (FD) > 0.5 mm were censored, and participants retaining fewer than 60 volumes were excluded. Head-motion parameters and mean white-matter and cerebrospinal-fluid signals were regressed. Data were smoothed with a 6-mm isotropic full-width-at-half-maximum Gaussian kernel and band-pass filtered (0.01–0.08 Hz). Mean FD was calculated for statistical adjustment.

The brain of each subjects were then normalized to an MNI template using the default unified segmentation method of SPM12. The Automated Anatomical Labeling atlas (AAL1) parcellated each brain into 90 regions [32], by using the built-in registration method in uRP platform [11]. Regional mean BOLD time series defined nodes, and pairwise Pearson correlations defined edges, yielding a 90 x 90 functional connectivity matrix.The Automated Anatomical Labeling atlas (AAL1) parcellated each brain into 90 regions [32], by using the built-in registration method in uRP platform [11]. Regional mean BOLD time series defined nodes, and pairwise Pearson correlations defined edges, yielding a 90 × 90 functional connectivity matrix.

Networks comprised the strongest 10% of positive connections. Global measures included global efficiency, mean local efficiency, mean clustering coefficient, and the rich-club coefficient. Rich-club, feeder, and local connectivity were also quantified. Nodal measures included degree, local efficiency, and clustering coefficient. Higher local efficiency and clustering indicate more efficient, robust neighborhood communication. Global efficiency was the prespecified primary outcome.

Statistical analysis

Participants were grouped by total CSVD burden (0–1, 2, and 3–4) for descriptive comparisons. Continuous data were summarized as mean (standard deviation) or median [first, third quartile], and categorical data as number (percentage). The SPSS version 24.0 (IBM Corp.) is utilized to analyze the group comparisons of non-imaging data. Group comparisons used one-way analysis of variance, Kruskal-Wallis tests, or Pearson chi-square tests as appropriate; age-adjusted group effects were also reported.

The primary multivariable ordinary least-squares model regressed global efficiency on continuous total CSVD burden, clinical acute infarction, age, sex, hypertension, diabetes mellitus, and meanFD. HC3 heteroskedasticity-robust standard errors, 95% confidence intervals (CIs), and two-sided P values were used. Four regional models separately added joint blocks of lacunes (frontal, parietal, and deep), CMBs (frontal, parietal, temporal, deep, and infratentorial), PVS volumes (six regions), or WMH volumes (four layers) to the same covariates. Low-frequency regions were excluded prospectively from the joint regional models. Benjamini-Hochberg false discovery rate (FDR) correction was applied within each lesion family.

Regional contribution was described using drop-one partial R-squared and exact Lindeman-Merenda-Gold/Shapley (LMG) decomposition of the incremental regional R-squared. Participant-level bootstrap resampling (1,000 samples; seed 20260801) estimated percentile 95% CIs and first-rank frequencies. A region could be called the largest contributor only if it had a negative coefficient, ranked first for both partial R-squared and LMG, ranked first in at least 70% of bootstrap samples, remained directionally stable, and showed supportive between-region LMG-difference intervals. Prespecified sensitivity analyses considered alternative acute-infarct volume definitions, the no-acute-infarct subgroup, global mean signal, retained time points instead of meanFD, a quadratic meanFD term, robust regression, influence diagnostics, and WMH collinearity. Regression and regional contribution analyses were performed using custom-written Python scripts (Python 3.12.13), with NumPy 2.3.5 and pandas 3.0.1 used for numerical computation and data management, respectively.

Results

Participant characteristics

The 166 participants had a mean age of 67.16 years (SD 9.40), 95 (57.2%) were men, 124 (74.7%) had hypertension, and 42 (25.3%) had diabetes mellitus. Clinical acute infarction was present in 80 (48.2%). Total CSVD burden scores were 0 in 39, 1 in 48, 2 in 33, 3 in 31, and 4 in 15 participants. Mean global efficiency was 0.4097 (SD 0.0273). The median global efficiency declined from 0.42 in the burden 0-1 group to 0.41 in the burden 3-4 group (unadjusted P=0.008; age-adjusted P=0.038), whereas the other five network measures did not differ significantly across burden groups (Table 1).

Total burden, acute infarction, and head motion

In the primary HC3 multivariable model, every 1-point increase in total CSVD burden was associated with a 0.0055 decrease in global efficiency (B=−0.0055, 95% CI: −0.0086 - 0.0024; P<0.001; standardized beta=−0.258) (Table 2). MeanFD was independently associated with lower global efficiency (B=−0.0731, 95% CI: −0.1293 - −0.0168; P=0.011). Clinical acute infarction was not independently associated with global efficiency (B=0.0008, 95% CI: −0.0071 - 0.0087; P=0.850). The model explained 24.3% of outcome variance (adjusted R-squared=0.209). Marginal-standardized predictions demonstrated an approximately linear decrease in adjusted global efficiency across burden scores 0-4 (Figure 3). Adding meanFD to the demographic and vascular-risk reference model increased R-squared by 0.1403 (robust P=0.015).

Regional CSVD models

The lacune regional block added 9.27% explained variance beyond clinical covariates, meanFD, and acute infarction (robust block P=0.00195). Parietal lacunes (B=−0.0130, 95% CI: −0.0237 - −0.0023; FDR q=0.026) and deep lacunes (B=−0.0132, 95% CI: −0.0228 - −0.0036; FDR q=0.021) were independently associated with lower global efficiency (Table 3; Figure 2A). Frontal lacunes were not associated. The CMB (block P=0.392), PVS (P=0.987), and WMH (P=0.057) blocks were not statistically significant; the WMH result was therefore considered only borderline and exploratory. The corresponding incremental R-squared values were 0.0344 for CMBs, 0.0057 for PVS, and 0.0413 for WMH.

Deep lacunes had the largest point estimate for LMG contribution within the lacune family, but ranked first in only 64.1% of bootstrap samples, below the prespecified 70% threshold (Figure 2B). Thus, the data did not support a claim that deep lacunes contributed significantly more than parietal lacunes.

Sensitivity analyses

Across prespecified sensitivity analyses, alternative clinical and imaging definitions of acute infarction, including volume-based models, did not produce an independent association with global efficiency. The negative parietal and deep lacune estimates were generally maintained across robust regression, influence-point, head-motion, global mean signal, and leave-one-out analyses; in the no-acute-infarction subgroup, the deep-lacune association remained significant, whereas the parietal estimate remained

negative but less precise. CMB and PVS blocks remained non-significant, and the WMH block remained borderline. Model diagnostics supported HC3 inference, and all bootstrap resamples completed successfully (Supplementary Tables S1-S3). In exploratory unadjusted analyses, higher total CSVD burden, lacune count, lacune volume, and RSSI count were correlated with lower global efficiency (Spearman rho=−0.24 - −0.25; all FDR $q<0.05$), whereas no correlations with the other network measures survived FDR correction (Figure S1).

Discussion

In this mixed cohort of acute and chronic cerebrovascular disease, greater cumulative CSVD burden was independently associated with lower resting-state functional global efficiency after adjustment for demographic factors, hypertension, diabetes, clinical acute infarction, and head motion. The regional analyses further identified the lacune block, particularly parietal and deep lacunes, as the most informative lesion family. By contrast, clinical acute infarction status showed no independent association, and the regional CMB, PVS, and WMH blocks were not significant. These findings support a cross-sectional link between chronic small-vessel injury and impaired large-scale functional integration, but they do not establish that chronic injury has a larger causal effect than acute infarction.

The association between total CSVD burden and global efficiency is biologically plausible because the burden score captures coexisting injury across several tissue compartments rather than a single imaging phenotype. CSVD is increasingly viewed as a whole-brain disorder in which focal lesions coexist with diffuse white-matter and microstructural injury [1, 4]. Structural network studies have consistently linked reduced efficiency to cognitive impairment and longitudinal decline [16, 17]. Functional network findings are less uniform, but altered centrality and connectivity of frontoparietal hubs have been reported in early CSVD [20], and reduced subsystem efficiency has been observed in cohorts with high inherited SVD burden [22]. Our adjusted marginal predictions suggest a graded relationship across scores 0–4 rather than a threshold effect, although the ordinal burden score cannot resolve which biological process drives this trend.

The location-specific lacune result adds anatomical detail. Parietal association cortex participates in multimodal integration and distributed control networks, while deep perforator territories contain compact projection and association pathways. Lacunes in these locations may therefore coincide with interruption of strategically important network routes even when lesion volume is small. Prior work has shown that the clinical and cognitive consequences of lacunes depend on location and connected circuitry [13]. Nevertheless, our contribution analysis did not meet the stringent criterion for declaring one region dominant: deep lacunes ranked first in 64.1% of bootstrap samples, and uncertainty in between-region differences remained. The defensible interpretation is that both parietal and deep lacunes were associated with lower global efficiency, not that one was demonstrably stronger.

The non-significant acute-infarction coefficient should be interpreted as a limitation of the binary acute-state contrast rather than evidence that acute ischemic injury has no network effect. First, the acute

response may not be a monotonic reduction in global efficiency. In patients with proximal anterior-circulation occlusion scanned within 12 hours, Zhu et al. observed higher global efficiency and shorter path length than in healthy controls, a pattern interpreted as greater network randomization [29]. Thus, lesion-driven disconnection, transient hyperconnectivity, and compensatory recruitment may exert opposing effects on a single global metric and attenuate the mean difference between patients with and without acute infarction. Second, network abnormalities evolve over time. Longitudinal scans obtained on days 1, 7, and 90 showed greater change in lesion-affected than unaffected networks, with network change related to clinical change [33]; another study found that dynamic connectivity states measured 2–5 days after stroke varied with acute severity and subsequent recovery [34]. Pooling patients across different post-onset intervals can therefore obscure phase-specific effects. Third, acute network disruption depends on where an infarct is embedded in the connectome, not simply whether an infarct is present. In 41 patients with acute ischemic stroke, the number of rich-club regions affected and acute functional path length improved outcome models beyond age and lesion volume [35], supporting the importance of strategic topology. Our clinical indicator did not encode vascular territory, cortical involvement, network-hub intersection, reperfusion, neurological severity, or exact imaging time. The volume-based sensitivity analysis was also null, but 10 acute cases lacked usable volume and lesion volume alone cannot capture location, disconnection, or diaschisis. Finally, pre-existing CSVD may alter network reserve and the response to a new infarct; this potential interaction was not tested to avoid overfitting and multiplicity. Accordingly, our result indicates only that clinical acute-infarction status did not explain additional cross-sectional variation in global efficiency under the present model. It neither excludes heterogeneous acute network effects nor establishes that chronic CSVD has a greater causal influence.

Head motion was a major analytical consideration. MeanFD was independently associated with global efficiency and explained substantial additional variance beyond the clinical covariates. Motion can systematically alter resting-state correlations and graph metrics, particularly in older or neurologically impaired participants [36]. Excluding participants with fewer than 60 retained time points and adjusting for meanFD reduced, but cannot eliminate, residual motion-related bias.

The CMB and PVS regional blocks were null, while the joint WMH block was borderline. These results should not be read as evidence that these markers lack biological relevance. Regional predictors were correlated, several lesion locations were uncommon, and the sample was modest for simultaneous multi-region models. WMH layers in particular showed collinearity, making individual coefficients unstable; single-layer and ridge sensitivity models were therefore treated as supportive rather than confirmatory. Quantitative segmentation improves lesion measurement, but differences in segmentation performance, lesion definitions, and anatomical assignment may still influence region-level estimates [11]. Recent population data further associate high regional PVS burden with lower structural network efficiency [37].

Limitations

Several limitations merit emphasis. First, the sample was relatively small, hospital based, and lacked healthy controls, limiting precision and generalizability. Second, the cross-sectional design precludes temporal or causal inference. Third, brain atrophy was not quantified and may confound relationships between vascular lesions and network topology. Fourth, acute infarcts were heterogeneous in location, volume, severity, and disease stage, and 10 clinically acute cases lacked usable RSSI volume for the volume-based sensitivity model. Finally, low-frequency lacune and CMB regions were excluded from joint models, reducing anatomical coverage.

Conclusions

Higher total CSVD burden was independently associated with lower resting-state functional global efficiency in patients with cerebrovascular disease. Parietal and deep lacunes showed region-specific negative associations, whereas no independent association was observed for clinical acute infarction status in this sample. These findings provide exploratory cross-sectional evidence that cumulative and strategically located small-vessel injury relates to impaired functional network integration and warrant longitudinal validation with complete acute-lesion characterization, atrophy and cognitive measures.

Declarations

Acknowledgements

We would like to thank all individuals who participated in this study and provided valuable data and assistance.

Funding

This research was supported by the National Nature Science Foundation of China (NSFC, No. 82371940) and the Fundamental Research Funds for the Central Universities (3290002503).

Ethics approval and consent to participate

This study was performed in accordance with the ethical principles of the Declaration of Helsinki. The protocol was approved by the Lianyungang First People's Hospital Medical Ethics Committee (approval no. KY-20231023001-01). The requirement for written informed consent was waived in accordance with applicable national legislation and institutional requirements.

Consent for publication

Not applicable.

Availability of data and materials

The raw data supporting the conclusions of this article will be made available by the authors, without undue reservation.

Competing interests

The authors declare no competing interests.

Clinical trial number

Not applicable.

Authors' contributions

Y.G: data curation, writing review and editing. C.L: data curation, writing review and editing. Y.L: validation, visualization, writing review and editing. Y.Z: validation, writing review and editing. L.Z: data curation, writing review and editing. Y.G: validation, conceptualization, supervision.

Authors' information

1 Department of Radiology, Lianyungang Clinical College of Nanjing Medical University, Lianyungang Jiangsu, China.

2 Nurturing Center of Jiangsu Province for State Laboratory of AI Imaging & Interventional Radiology, Department of Radiology, Zhongda Hospital, Medical School of Southeast University, 87 Dingjiaqiao Road, Nanjing, Jiangsu 210009, China.

References

1. Duering M, Biessels GJ, Brodtmann A, et al. Neuroimaging standards for research into small vessel disease-advances since 2013. Lancet Neurol. 2023;22:602–618. doi:10.1016/S1474-4422(23)00131-X.
2. Doubal FN, MacLullich AMJ, Ferguson KJ, Dennis MS, Wardlaw JM. Enlarged perivascular spaces on MRI are a feature of cerebral small vessel disease. Stroke. 2010;41:450–454. doi:10.1161/STROKEAHA.109.564914.
3. Rodriguez Lara F, Toro AR, Pinheiro A, et al. Relation of MRI-visible perivascular spaces and other MRI markers of cerebral small vessel disease. Brain Sci. 2023;13:1323. doi:10.3390/brainsci13091323.
4. Wardlaw JM, Smith C, Dichgans M. Small vessel disease: mechanisms and clinical implications. Lancet Neurol. 2019;18:684–696. doi:10.1016/S1474-4422(19)30079-1.
5. Mooldijk SS, Ikram MA. Cerebral small vessel disease in population-based research: what are we looking at-and what not? Aging Dis. 2024;15:1438–1446. doi:10.14336/AD.2023.0323.
6. Ter Telgte A, Duering M. Cerebral small vessel disease: advancing knowledge with neuroimaging. Stroke. 2024;55:1686–1688. doi:10.1161/STROKEAHA.123.044294.
7. Kilinc D, Vernooij MW, Bron EE, Biessels GJ, Vinke EJ. Normative population-derived data for MRI manifestations of cerebral small vessel disease. Stroke. 2024;55:2863–2871.

doi:10.1161/STROKEAHA.124.046731.

8. Sperber C, Hakim A, Gallucci L, et al. A typology of cerebral small vessel disease based on imaging markers. J Neurol. 2023;270:4985–4994. doi:10.1007/s00415-023-11831-x.
9. Staals J, Makin SDJ, Doubal FN, Dennis MS, Wardlaw JM. Stroke subtype, vascular risk factors, and total MRI brain small-vessel disease burden. Neurology. 2014;83:1228–1234. doi:10.1212/WNL.0000000000000837.
10. Silva GD, Telles JPM, Rimkus CM, et al. Reliability and validity of the total cerebral small vessel disease score: a systematic review and meta-analysis. Front Neurol. 2025;16:1593402. doi:10.3389/fneur.2025.1593402.
11. Zhang Z, Ding Z, Chen F, et al. Quantitative analysis of multimodal MRI markers and clinical risk factors for cerebral small vessel disease based on deep learning. Int J Gen Med. 2024;17:739–750. doi:10.2147/IJGM.S446531.
12. Lu CQ, Liu Y, Huang JR, et al. Quantitative comparison of CSVD imaging markers between patients with possible amyloid small vessel disease and with non-amyloid small vessel disease. Neuroimage Clin. 2024;44:103681. doi:10.1016/j.nicl.2024.103681.
13. Benjamin P, Lawrence AJ, Lambert C, Patel B, Chung AW, MacKinnon AD, et al. Strategic lacunes and their relationship to cognitive impairment in cerebral small vessel disease. Neuroimage Clin. 2014;4:828–837. doi:10.1016/j.nicl.2014.05.009.
14. Petersen M, Coenen M, DeCarli C, et al. Enhancing cognitive performance prediction by white matter hyperintensity connectivity assessment. Brain. 2024;147:4265–4279. doi:10.1093/brain/awae315.
15. Bullmore E, Sporns O. Complex brain networks: graph theoretical analysis of structural and functional systems. Nat Rev Neurosci. 2009;10:186–198. doi:10.1038/nrn2575.
16. Lawrence AJ, Chung AW, Morris RG, Markus HS, Barrick TR. Structural network efficiency is associated with cognitive impairment in small-vessel disease. Neurology. 2014;83:304–311. doi:10.1212/WNL.0000000000000612.
17. Tuladhar AM, van Dijk E, Zwiers MP, et al. Structural network connectivity and cognition in cerebral small vessel disease. Hum Brain Mapp. 2016;37:300–310. doi:10.1002/hbm.23032.
18. Boot EM, Mc van Leijsen E, Bergkamp MI, et al. Structural network efficiency predicts cognitive decline in cerebral small vessel disease. Neuroimage Clin. 2020;27:102325. doi:10.1016/j.nicl.2020.102325.
19. Tuladhar AM, Tay J, van Leijsen EMC, et al. Structural network changes in cerebral small vessel disease. J Neurol Neurosurg Psychiatry. 2020;91:196–203. doi:10.1136/jnnp-2019-321767.
20. Schaefer A, Quinque EM, Kipping JA, et al. Early small vessel disease affects frontoparietal and cerebellar hubs in close correlation with clinical symptoms-a resting-state fMRI study. J Cereb Blood Flow Metab. 2014;34:1091–1095. doi:10.1038/jcbfm.2014.70.
21. Qin Y, Zhu W, Liu C, Wang Z, Zhu W. Functional brain connectome and its relation to mild cognitive impairment in cerebral small vessel disease patients with thalamus lacunes: a cross-sectional study. Medicine (Baltimore). 2019;98:e17127. doi:10.1097/MD.0000000000017127.

22. Gesierich B, Tuladhar AM, ter Telgte A, et al. Alterations and test-retest reliability of functional connectivity network measures in cerebral small vessel disease. Hum Brain Mapp. 2020;41:2629–2641. doi:10.1002/hbm.24967.
23. Lawrence AJ, Tozer DJ, Stamatakis EA, Markus HS. A comparison of functional and tractography based networks in cerebral small vessel disease. Neuroimage Clin. 2018;18:425–432. doi:10.1016/j.nicl.2018.02.013.
24. Schulz M, Malherbe C, Cheng B, Thomalla G, Schlemm E. Functional connectivity changes in cerebral small vessel disease-a systematic review of the resting-state MRI literature. BMC Med. 2021;19:103. doi:10.1186/s12916-021-01962-1.
25. Liu R, Chen H, Qin R, et al. The altered reconfiguration pattern of brain modular architecture regulates cognitive function in cerebral small vessel disease. Front Neurol. 2019;10:324. doi:10.3389/fneur.2019.00324.
26. Xin H, Wen H, Feng M, et al. Disrupted topological organization of resting-state functional brain networks in cerebral small vessel disease. Hum Brain Mapp. 2022;43:2607–2620. doi:10.1002/hbm.25808.
27. Yi LY, Liang X, Liu DM, et al. Disrupted topological organization of resting-state functional brain network in subcortical vascular mild cognitive impairment. CNS Neurosci Ther. 2015;21:846–854. doi:10.1111/cns.12424.
28. Chen X, Huang L, Ye Q, et al. Disrupted functional and structural connectivity within default mode network contribute to WMH-related cognitive impairment. Neuroimage Clin. 2019;24:102088. doi:10.1016/j.nicl.2019.102088.
29. Zhu Y, Bai L, Liang P, Kang S, Gao H, Yang H. Disrupted brain connectivity networks in acute ischemic stroke patients. Brain Imaging Behav. 2017;11:444–453. doi:10.1007/s11682-016-9525-6.
30. Paradise MB, Beaudoin MS, Dawes L, et al. Development and validation of a rating scale for perivascular spaces on 3T MRI. J Neurol Sci. 2020;409:116621. doi:10.1016/j.jns.2019.116621.
31. Wu J, Xia Y, Wang X, Wei Y, Liu A, Innanje A, et al. uRP: An integrated research platform for one-stop analysis of medical images. Front Radiol. 2023;3:1153784. doi:10.3389/fradi.2023.1153784.
32. Tzourio-Mazoyer N, Landeau B, Papathanassiou D, et al. Automated anatomical labeling of activations in SPM using a macroscopic anatomical parcellation of the MNI MRI single-subject brain. Neuroimage. 2002;15:273–289. doi:10.1006/nimg.2001.0978.
33. Ovadia-Caro S, Villringer K, Fiebach J, et al. Longitudinal effects of lesions on functional networks after stroke. J Cereb Blood Flow Metab. 2013;33:1279–1285. doi:10.1038/jcbfm.2013.80.
34. Bonkhoff AK, Schirmer MD, Bretzner M, et al. Abnormal dynamic functional connectivity is linked to recovery after acute ischemic stroke. Hum Brain Mapp. 2021;42:2278–2291. doi:10.1002/hbm.25366.
35. Ktena SI, Schirmer MD, Etherton MR, et al. Brain connectivity measures improve modeling of functional outcome after acute ischemic stroke. Stroke. 2019;50:2761–2767. doi:10.1161/STROKEAHA.119.025738.

36. Power JD, Mitra A, Laumann TO, Snyder AZ, Schlaggar BL, Petersen SE. Methods to detect, characterize, and remove motion artifact in resting state fMRI. Neuroimage. 2014;84:320–341. doi:10.1016/j.neuroimage.2013.08.048.
37. Ekenze O, Seiler S, Pinheiro A, et al. Relation of MRI visible perivascular spaces with global and regional brain structural connectivity measures: The Framingham Heart Study. Neurobiol Aging. 2025;150:1–8. doi:10.1016/j.neurobiolaging.2025.02.007.

Tables

Table 1. Clinical, CSVD imaging, and brain network characteristics according to CSVD burden

Characteristic	Data presentation	CSVD burden 0–1 (n=87)	CSVD burden 2 (n=33)	CSVD burden 3–4 (n=46)	Unadjusted P value	Age-adjusted P value
Demographic and clinical characteristics						
Age, years	Mean (SD)	65.83 (9.21)	66.06 (8.97)	70.48 (9.43)	0.018	—
Male sex	n (%)	51 (58.6)	16 (48.5)	28 (60.9)	0.509	0.380
Acute infarction	n (%)	40 (46.0)	17 (51.5)	23 (50.0)	0.828	0.642
Hypertension	n (%)	60 (69.0)	26 (78.8)	38 (82.6)	0.189	0.255
Diabetes mellitus	n (%)	22 (25.3)	9 (27.3)	11 (23.9)	0.944	0.968
Mean framewise displacement	Median [Q1, Q3]	0.21 [0.15, 0.29]	0.16 [0.12, 0.21]	0.16 [0.13, 0.28]	0.137	0.188
CSVD imaging markers						
Number of lacunes	Median [Q1, Q3]	0.00 [0.00, 0.00]	1.00 [0.00, 2.00]	2.00 [1.00, 4.75]	<0.001	<0.001
Total lacune volume, mm^3	Median [Q1, Q3]	0.00 [0.00, 0.00]	111.40 [0.00, 214.54]	240.33 [85.09, 630.21]	<0.001	<0.001
Juxtaventricular WMH volume, cm^3	Median [Q1, Q3]	3.34 [2.25, 5.60]	5.43 [4.63, 8.24]	9.77 [6.65, 13.89]	<0.001	<0.001
Periventricular WMH volume, cm^3	Median [Q1, Q3]	1.60 [0.71, 3.84]	7.48 [3.21, 12.34]	18.23 [8.51, 31.94]	<0.001	<0.001
Deep WMH volume, cm^3	Median [Q1, Q3]	0.83 [0.47, 1.63]	1.59 [0.68, 4.03]	2.70 [1.33, 5.34]	<0.001	<0.001
Juxtacortical WMH volume, cm^3	Median [Q1, Q3]	0.31 [0.13, 0.81]	0.52 [0.34, 1.58]	1.01 [0.61, 1.93]	<0.001	<0.001
Periventricular WMH Fazekas score	Median [Q1, Q3]	1.00 [1.00, 2.00]	2.00 [2.00, 2.00]	2.00 [2.00, 2.00]	<0.001	<0.001

Characteristic	Data presentation	CSVD burden 0–1 (n=87)	CSVD burden 2 (n=33)	CSVD burden 3–4 (n=46)	Unadjusted P value	Age-adjusted P value
Deep WMH Fazekas score	Median [Q1, Q3]	1.00 [1.00, 1.00]	1.00 [1.00, 2.00]	2.00 [2.00, 2.00]	<0.001	<0.001
Number of PVS	Mean (SD)	143.30 (53.38)	169.82 (57.94)	144.74 (65.92)	0.072	0.074
Total PVS volume, mm^3	Mean (SD)	5051.27 (2627.02)	6134.22 (2991.98)	4769.31 (2968.20)	0.085	0.140
Number of RSSI	Median [Q1, Q3]	0.00 [0.00, 1.00]	0.00 [0.00, 1.00]	1.00 [0.00, 2.00]	0.571	0.688
Total RSSI volume, mm^3	Median [Q1, Q3]	0.00 [0.00, 1456.40]	0.00 [0.00, 2665.25]	119.65 [0.00, 1202.66]	0.932	0.368
Number of CMB	Median [Q1, Q3]	0.00 [0.00, 0.00]	1.00 [0.00, 2.00]	2.50 [1.00, 5.00]	<0.001	<0.001
Total CMB volume, mm^3	Median [Q1, Q3]	0.00 [0.00, 0.00]	11.30 [0.00, 73.46]	78.95 [19.40, 236.52]	<0.001	<0.001
Brain network measures						
Global efficiency	Median [Q1, Q3]	0.42 [0.41, 0.43]	0.42 [0.39, 0.43]	0.41 [0.39, 0.42]	0.008	0.038
Average local efficiency	Mean (SD)	0.61 (0.04)	0.62 (0.03)	0.62 (0.04)	0.352	0.167
Average clustering coefficient	Mean (SD)	0.45 (0.04)	0.45 (0.04)	0.46 (0.04)	0.317	0.096
Rich-club connectivity	Mean (SD)	29.26 (15.27)	31.28 (15.83)	33.16 (16.59)	0.391	0.316
Feeder connectivity	Mean (SD)	72.06 (15.76)	71.25 (12.13)	68.96 (15.54)	0.528	0.484
Local connectivity	Mean (SD)	110.49 (14.20)	108.17 (14.84)	109.51 (17.05)	0.750	0.719

Values are presented as mean (SD), median [Q1, Q3], or n (%), as appropriate.

Unadjusted P values were obtained using one-way ANOVA, Kruskal-Wallis tests, or Pearson chi-square tests, as appropriate.

Adjusted P values represent the overall CSVD-group effect after adjustment for age only. Continuous outcomes used OLS models with HC3 robust standard errors and a 2-df Wald test; binary outcomes used logistic regression with a 2-df likelihood-ratio test.

Age was not adjusted for itself. Sex and meanFD were reported but were not included as adjustment covariates in this analysis.

Abbreviations: CMB, cerebral microbleed; CSVD, cerebral small vessel disease; PVS, perivascular space; RSSI, recent small subcortical infarct; SD, standard deviation; WMH, white matter hyperintensity.

Table 2. Multivariable linear regression of global efficiency in the final cohort

Predictor	B	Robust SE	95% CI	Standardized β	t	P value	VIF
Intercept	0.4180	0.0161	0.3861 - 0.4499	—	25.888	<0.001	—
Acute infarction	0.0008	0.0040	-0.0071 - 0.0087	0.028	0.190	0.850	1.21
Age	0.0002	0.0002	-0.0003 - 0.0007	0.064	0.774	0.440	1.11
Male sex	-0.0035	0.0042	-0.0117 - 0.0048	-0.127	-0.828	0.409	1.17
Hypertension	0.0073	0.0049	-0.0024 - 0.0171	0.269	1.482	0.140	1.09
Diabetes mellitus	0.0045	0.0039	-0.0032 - 0.0123	0.167	1.163	0.247	1.04
CSVD burden	-0.0055	0.0015	-0.0086 - -0.0024	-0.258	**-3.548**	**<0.001**	1.09
Mean framewise displacement	-0.0731	0.0285	-0.1293 - -0.0168	-0.410	-2.566	0.011	1.09

Model summary: N=166; R^2=0.243; adjusted R^2=0.209; F(7, 158)=7.245, P<0.001; RMSE=0.0242; AIC=-756.01; BIC=-731.11.

B values are unstandardized regression coefficients. SEs, 95% CIs, t statistics, and P values are based on HC3 heteroskedasticity-robust covariance estimates.

Standardized β was calculated after standardizing the outcome and continuous predictors; binary predictors remained coded 0/1.

Coding: acute infarction, yes=1/no=0; male sex, male=1/female=0; hypertension and diabetes mellitus, yes=1/no=0; CSVD burden was modeled as a continuous score (0–4).

Abbreviations: AIC, Akaike information criterion; BIC, Bayesian information criterion; CI, confidence interval; CSVD, cerebral small vessel disease; HC3, heteroskedasticity-consistent covariance estimator; RMSE, root mean square error; SE, standard error; VIF, variance inflation factor.

Table 3. Regional CSVD markers associated with global efficiency in multivariable HC3 linear regression

Marker family	Regional predictor	B (95% CI)	P value	FDR q value
LA	Frontal lacune	0.0014 (-0.0084 - 0.0113)	0.772	0.772
LA	Parietal lacune	-0.0130 (-0.0237 - -0.0023)	**0.017**	**0.026**
LA	Deep lacune	-0.0132 (-0.0228 - -0.0036)	**0.007**	**0.021**
CMB	Frontal CMB	0.0023 (-0.0107 - 0.0152)	0.731	0.731
CMB	Parietal CMB	-0.0060 (-0.0215 - 0.0096)	0.450	0.731
CMB	Temporal CMB	-0.0046 (-0.0154 - 0.0062)	0.399	0.731
CMB	Deep CMB	-0.0070 (-0.0195 - 0.0055)	0.272	0.731
CMB	Infratentorial CMB	-0.0034 (-0.0175 - 0.0106)	0.629	0.731
PVS	Frontal PVS volume	0.0001 (-0.0078 - 0.0080)	0.979	0.979
PVS	Parietal PVS volume	0.0019 (-0.0049 - 0.0088)	0.578	0.979
PVS	Temporal PVS volume	-0.0009 (-0.0077 - 0.0058)	0.785	0.979
PVS	Occipital PVS volume	-0.0004 (-0.0055 - 0.0047)	0.885	0.979
PVS	Deep PVS volume	-0.0018 (-0.0067 - 0.0031)	0.474	0.979
PVS	Infratentorial PVS volume	0.0003 (-0.0036 - 0.0042)	0.882	0.979
WMH	Juxtaventricular WMH volume	0.0031 (-0.0080 - 0.0142)	0.580	0.773
WMH	Periventricular WMH volume	-0.0062 (-0.0179 - 0.0055)	0.297	0.683
WMH	Deep WMH volume	0.0001 (-0.0060 - 0.0061)	0.986	0.986
WMH	Juxtacortical WMH volume	-0.0028 (-0.0087 - 0.0030)	0.341	0.683

Each marker family was analyzed in a separate model adjusted for age, sex, hypertension, diabetes mellitus, mean framewise displacement, and clinical acute infarction. PVS and WMH volumes were ln(volume + 1) transformed and standardized within the final cohort. FDR q values used Benjamini-Hochberg correction within each marker family.

Excluded low-frequency regions: occipital lacune, 3 positive participants; infratentorial lacune, 6 positive participants; temporal lacune, 7 positive participants; occipital CMB, 8 positive participants.
Abbreviations: CI, confidence interval; CMB, cerebral microbleed; CSVD, cerebral small vessel disease; FDR, false discovery rate; LA, lacune; PVS, perivascular space; WMH, white matter hyperintensity.

Figures

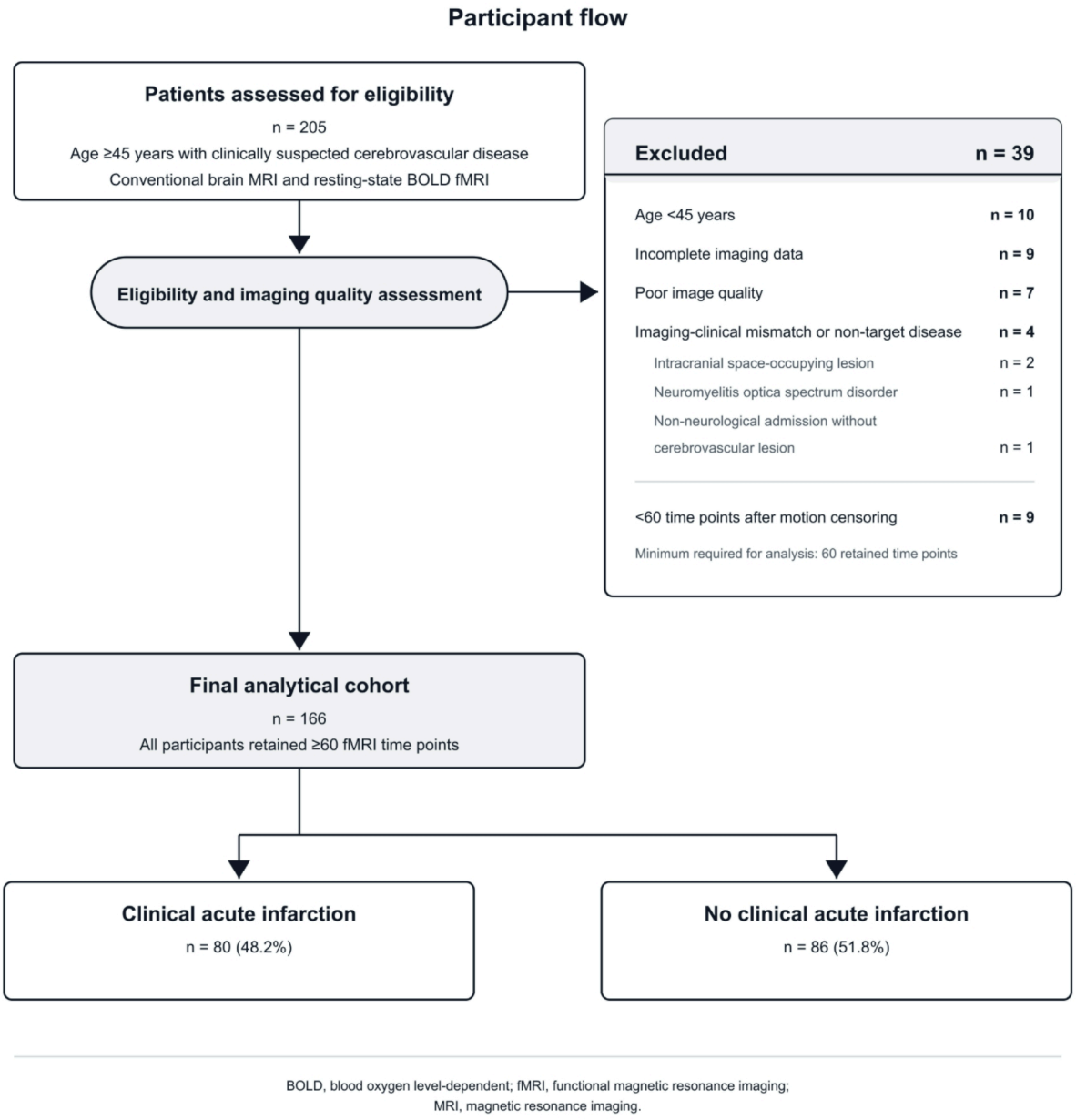

Figure 1

Participant flow diagram. Thirty-nine of 205 screened patients were excluded, leaving 166 participants for analysis. BOLD, blood oxygen level-dependent; fMRI, functional magnetic resonance imaging; MRI, magnetic resonance imaging.

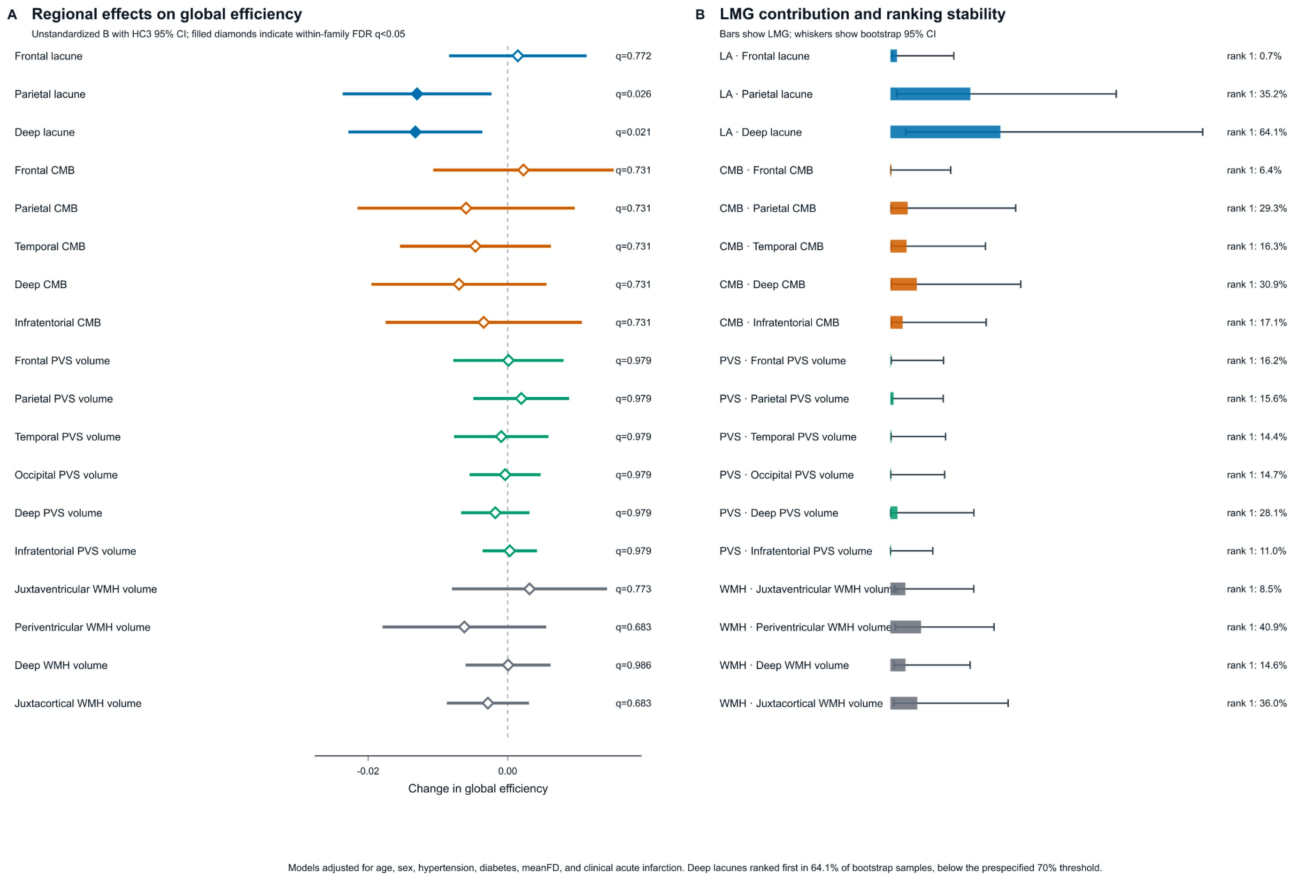

Figure 2

Regional associations with global efficiency and relative contribution. (A) Unstandardized coefficients and HC3 95% CIs from four separate regional multivariable models; filled diamonds indicate within-family FDR q<0.05. (B) LMG decomposition of regional incremental R-squared with bootstrap 95% CIs and first-rank frequency. Deep lacunes ranked first in 64.1% of bootstrap samples, below the prespecified 70% threshold. All models adjusted for age, sex, hypertension, diabetes mellitus, meanFD, and clinical acute infarction.

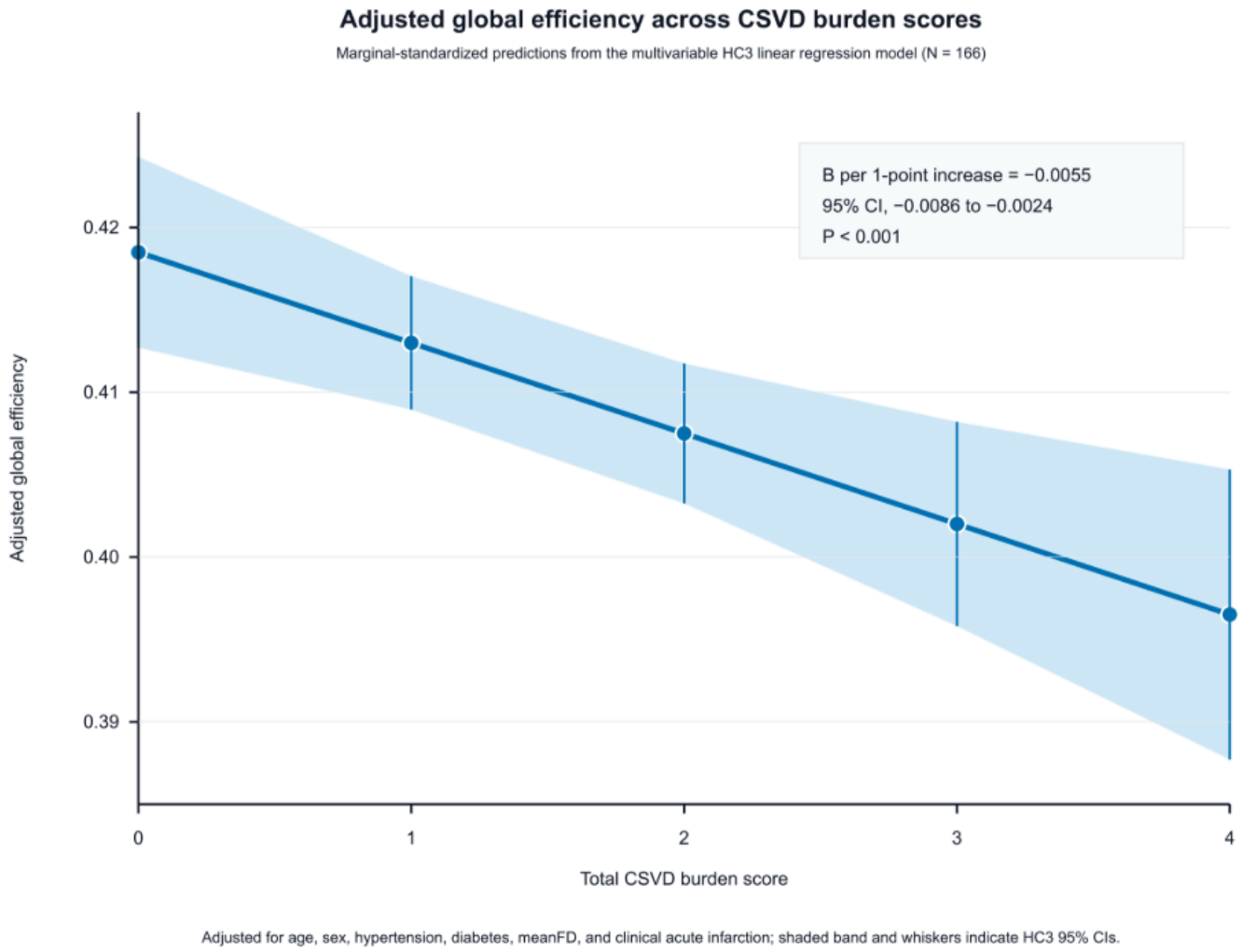

Figure 3

Marginal-standardized global efficiency across total CSVD burden scores. Predictions were calculated from the Table 2 model and averaged over the observed covariate distribution in 166 participants. The band and whiskers show HC3 95% CIs.

Supplementary Files

This is a list of supplementary files associated with this preprint. Click to download.

- Supplementarymaterialv1.docx